Time-resolved interferometry of femtosecond-laser-induced processes under tight focusing and close-to-optical breakdown inside borosilicate glass

Yoshio Hayasaki,[1,*] Mitsuhiro Isaka,[1] Akihiro Takita,[1] and Saulius Juodkazis[2]

[1]*Center for Optical Research and Education (CORE), Utsunomiya University, 7-1-2 Yoto, Utsunomiya 321-8585, Japan*

[2]*Centre for Micro-Photonics, Faculty of Engineering and Industrial Sciences, Swinburne University of Technology, Hawthorn, VIC, 3122, Australia*

**hayasaki@opt.utsunomiya-u.ac.jp*

Abstract: We use an interferometric time-resolved observation of a femtosecond-laser pulse (800nm/45fs) interaction with glass from 100 fs to 10 ns at spatial lateral resolution down to the wavelength of the pulse. The phase and amplitude images reveal sequence of events after the irradiation of a single ultra-short laser pulse at close-to-threshold intensity when permanent refractive index changes occur. The proposed method is applicable to characterization of the processes induced by tightly focused fs-laser pulses during three-dimensional structuring of glasses and crystals for fundamental studies and optical applications. Generation of carriers, thermal expansion, generation and propagation of shockwaves, and formation of refractive index changes are experimentally observed and resolved in time and space with the highest resolution. Quantitative estimations of the threshold energies of different processes are achieved. The threshold energy of carrier generation is found the same as that of shockwave generation while the threshold energy of refractive index changes was by 40% higher. Application potential of the method is discussed.

©2011 Optical Society of America

OCIS codes: (140.3391) Laser materials processing; (120.3180) Interferometry; (320.7120) Ultrafast phenomena; (220.4241) Nanostructure fabrication.

References and links

1. C. E. Bell, and J. A. Landt, "Laser-induced high-pressure shock waves in water," Appl. Phys. Lett. **10**(2), 46–48 (1967).
2. D. C. Emmony, M. Siegrist, and F. K. Kneubühl, "Laser-induced shock waves in liquids," Appl. Phys. Lett. **29**(9), 547–549 (1976).
3. A. Vogel, S. Busch, and U. Parlitz, "Shock wave emission and cavitation bubble generation by picosecond and nanosecond optical breakdown in water," J. Acoust. Soc. Am. **100**(1), 148–165 (1996).
4. C. B. Schaffer, N. Nishimura, E. N. Glezer, A. M.-T. Kim, and E. Mazur, "Dynamics of femtosecond laser-induced breakdown in water from femtoseconds to microseconds," Opt. Express **10**(3), 196–203 (2002).
5. E. Abraham, K. Minoshima, and H. Matsumoto, "Femtosecond laser-induced breakdown in water: time-resolved shadow imaging and two-color interferometric imaging," Opt. Commun. **176**(4-6), 441–452 (2000).
6. X. Zeng, X. Mao, S. S. Mao, A.-B. Wen, R. Greif, and E. Russo, "Laser-induced shockwave propagation from ablation in a cavity," Appl. Phys. Lett. **88**(6), 061502 (2006).
7. X. Zeng, X. L. Mao, R. Greif, and R. E. Russo, "Experimental investigation of ablation efficiency and plasma expansion during femtosecond and nanosecond laser ablation on silicon," Appl. Phys., A Mater. Sci. Process. **80**(2), 237–241 (2005).
8. R. Petkovšek, and P. Gregorčič, "A laser probe measurement of cavitation bubble dynamics improved by shock wave detection and compared to shadow photography," J. Appl. Phys. **102**(4), 044909 (2007).
9. W. Gawelda, D. Puerto, J. Siegel, A. Ferrer, A. Ruiz de la Cruz, H. Fernández, and J. Solis, "Ultrafast imaging of transient electronic plasmas produced in conditions of femtosecond waveguide writing in dielectrics," Appl. Phys. Lett. **93**(12), 121109 (2008).
10. A. Gopal, S. Minardi, and M. Tatarakis, "Quantitative two-dimensional shadowgraphic method for high-sensitivity density measurement of under-critical laser plasmas," Opt. Lett. **32**(10), 1238–1240 (2007).

#139857 - $15.00 USD Received 20 Dec 2010; revised 14 Feb 2011; accepted 28 Feb 2011; published 14 Mar 2011

11. Q. Sun, H. Jiang, Y. Liu, Z. Wu, H. Yang, and Q. Gong, "Measurement of the collision time of dense electronic plasma induced by a femtosecond laser in fused silica," Opt. Lett. **30**(3), 320–322 (2005).
12. V. V. Temnov, K. Sokolowski-Tinten, P. Zhou, and D. von der Linde, " "Ultrafast imaging interferometry at femtosecond-laser-excited surfaces," J. Opt. Soc. Am. B **23**(9), 1954–1964 (2006).
13. A. Takita, and Y. Hayasaki, "Interference measurement of superposition of laser-induced shock waves in water," Jpn. J. Appl. Phys. **48**(9), 09LD04 (2009).
14. Z. Liu, G. J. Steckman, and D. Psaltis, "Holographic recording of fast phenomena," Appl. Phys. Lett. **80**(5), 731–733 (2002).
15. M. Centurion, Y. Pu, Z. Liu, D. Psaltis, and T. W. Hänsch, "Holographic recording of laser-induced plasma," Opt. Lett. **29**(7), 772–774 (2004).
16. X. Wang, H. Zhai, and G. Mu, "Pulsed digital holography system recording ultrafast process of the femtosecond order," Opt. Lett. **31**(11), 1636–1638 (2006).
17. T. Balciunas, A. Melninkaitis, G. Tamosauskas, and V. Sirutkaitis, "Time-resolved off-axis digital holography for characterization of ultrafast phenomena in water," Opt. Lett. **33**(1), 58–60 (2008).
18. S. Minardi, A. Gopal, M. Tatarakis, A. Couairon, G. Tamošauskas, R. Piskarskas, A. Dubietis, and P. Di Trapani, "Time-resolved refractive index and absorption mapping of light-plasma filaments in water," Opt. Lett. **33**(1), 86–88 (2008).
19. Y. Hayasaki, T. Sugimoto, A. Takita, and N. Nishida, "Variable holographic femtosecond laser processing by use of spatial light modulator," Appl. Phys. Lett. **87**(3), 031101 (2005).
20. J. Siegel, D. Puerto, W. Gawelda, G. Bachelier, J. Solis, L. Ehrentraut, and J. Bonse, "Plasma formation and structural modification below the visible ablation threshold in fused silica upon femtosecond laser irradiation," Appl. Phys. Lett. **91**(8), 082902 (2007).
21. A. Mermillod-Blondin, J. Bonse, A. Rosenfeld, I. V. Hertel, Yu. P. Meshcheryakov, N. M. Bulgakova, E. Audouard, and R. Stoian, "Dynamics of femtosecond laser induced voidlike structures in fused silica," Appl. Phys. Lett. **94**(4), 041911 (2009).
22. C. B. Schaffer, A. O. Jamison, and E. Mazur, "Morphology of femtosecond laser-induced structural changes in bulk transparent materials," Appl. Phys. Lett. **84**(9), 1441 (2004).
23. E. N. Glezer, M. Milosavljevic, L. Huang, R. J. Finlay, T.-H. Her, J. P. Callan, and E. Mazur, "Three-dimensional optical storage inside transparent materials," Opt. Lett. **21**(24), 2023–2025 (1996).
24. K. Yamasaki, S. Juodkazis, M. Watanabe, H.-B. Sun, S. Matsuo, and H. Misawa, "Recording by microexplosion and two photon reading of three dimensional optical memory in polymethylmethacrylate films," Appl. Phys. Lett. **76**(8), 1000–1002 (2000).
25. A. Takita, H. Yamamoto, Y. Hayasaki, N. Nishida, and H. Misawa, "Three-dimensional optical memory using a human fingernail," Opt. Express **13**(12), 4560–4567 (2005).
26. K. M. Davis, K. Miura, N. Sugimoto, and K. Hirao, "Writing waveguides in glass with a femtosecond laser," Opt. Lett. **21**(21), 1729–1731 (1996).
27. M. Ams, G. D. Marshall, D. J. Spence, and M. J. Withford, "Slit beam shaping method for femtosecond laser direct-write fabrication of symmetric waveguides in bulk glasses," Opt. Express **13**(15), 5676–5681 (2005).
28. N. Takeshima, Y. Narita, S. Tanaka, Y. Kuroiwa, and K. Hirao, "Fabrication of high-efficiency diffraction gratings in glass," Opt. Lett. **30**(4), 352–354 (2005).
29. H.-B. Sun, S. Matsuo, and H. Misawa, "Three-dimensional photonic crystal structures achieved with two-photon-absorption photopolymerization of resin," Appl. Phys. Lett. **74**(6), 786–788 (1999).
30. T. Kaji, S. Ito, H. Miyasaka, Y. Hosokawa, H. Masuhara, C. Shukunami, and Y. Hiraki, "Nondestructive micropatterning of living animal cells using focused femtosecond laser-induced impulsive force," Appl. Phys. Lett. **91**(2), 023904 (2007).
31. M. Takeda, H. Ina, and S. Kobayashi, "Fourier-transform method of fringe-pattern analysis for computer-based tomography and interferometry," J. Opt. Soc. Am. **72**(1), 156–160 (1982).
32. S. Juodkazis, K. Nishimura, S. Tanaka, H. Misawa, E. G. Gamaly, B. Luther-Davies, L. Hallo, P. Nicolai, and V. T. Tikhonchuk, "Laser-induced microexplosion confined in the bulk of a sapphire crystal: evidence of multimegabar pressures," Phys. Rev. Lett. **96**(16), 166101 (2006).
33. T. Hashimoto, S. Juodkazis, and H. Misawa, "Void formation in glasses," N. J. Phys. **9**(8), 253 (2007).
34. M. Shimizu, M. Sakakura, M. Ohnishi, Y. Shimotsuma, T. Nakaya, K. Miura, and K. Hirao, "Mechanism of heat-modification inside a glass after irradiation with high-repetition rate femtosecond laser pulses," J. Appl. Phys. **108**(7), 073533 (2010).
35. J. Morikawa, A. Orie, T. Hashimoto, and S. Juodkazis, "Thermal and optical properties of the femtosecond-laser-structured and stress-induced birefringent regions in sapphire," Opt. Express **18**(8), 8300–8310 (2010).
36. T. M. Gross, and M. Tomozawa, "Fictive temperature of GeO_2 glass: its determination by IR method and its effects on density and refractive index," J. Non-Cryst. Solids **353**(52-54), 4762–4766 (2007).
37. A. Mermillod-Blondin, I. M. Burakov, Yu. P. Meshcheryakov, N. M. Bulgakova, E. Audouard, A. Rosenfeld, A. Husakou, I. V. Hertel, and R. Stoian, "Flipping the sign of refractive index changes in ultrafast and temporally shaped laser-irradiated borosilicate crown optical glass at high repetition rates," Phys. Rev. B **77**(10), 104205 (2008).
38. L. Hallo, A. Bourgeade, V. T. Tikhonchuk, C. Mezel, and J. Breil, "Model and numerical simulations of the propagation and absorption of a short laser pulse in a transparent dielectric material: Blast-wave launch and cavity formation," Phys. Rev. B **76**(2), 024101 (2007).

#139857 - $15.00 USD Received 20 Dec 2010; revised 14 Feb 2011; accepted 28 Feb 2011; published 14 Mar 2011
(C) 2011 OSA

39. M. K. Bhuyan, F. Courvoisier, P. A. Lacourt, M. Jacquot, R. Salut, L. Furfaro, and J. M. Dudley, "High aspect ratio nanochannel machining using single shot femtosecond Bessel beams," Appl. Phys. Lett. **97**(8), 081102 (2010).

1. Introduction

Imaging of laser-induced spatiotemporal phenomena, including microplasmas, shockwaves, and cavitation bubbles, is very important to determine suitable irradiation conditions in femtosecond laser processing. An imaging by pump–probe shadowgraphy was applied to observe the temporal evolution of femtosecond-laser-induced phenomena inside dielectrics [1–10]. Other types of pump–probe observations using interferometry [5,11–13], digital holography [14–17], and modified shadowgraphy [18] have also been developed to obtain phase change distributions. The phase change indicates a refractive index modification in the media caused by a high-density plasma, a high-pressure shockwave, or a cavitation bubble, densification, and thermal expansion. We investigated the laser-induced phenomena in a parallel pump-probe geometry [13] because it is used in laser writing applications, which have to be improved in terms of fabrication throughput and efficiency of the light usage [19]. This geometry is applicable for in situ monitoring of light-matter interaction during direct laser writing.

Most of the previous studies on laser-induced phenomena were performed with low numerical aperture (NA) lens configurations; the maximum NA was 0.45 [20,21]. In the case of low-NA, it is possible to observe a side view of the laser-induced phenomena. However, the phenomena usually extend in the axial direction, and the axial and lateral resolutions of the processing are of micrometer order [22]. To realize nanofabrication [22] of optical memories [23–25], optical waveguides [26,27] and gratings [28] based on refractive-index modifications, three-dimensional photonic crystals [29], and biomaterials [30], we need to focus femtosecond laser pulses using a lens with a high-NA, typically 1.2-1.4, at the irradiation conditions near the threshold of a optical breakdown and plasma generation. However, time-resolved experiments of femtosecond laser-induced phenomena under conditions close to an optical breakdown using high-NA lens configurations have not been reported.

In this paper, we describe a detailed study of laser-induced phenomena in glass when a femtosecond laser pulse was tightly focused with a high-NA objective lens. A time-resolved pump–probe interference microscope acquired quantitative information of the temporal evolution of the processes with subpicosecond time resolution in the case of single-pulse irradiation. In addition, the high-NA configuration was capable of submicrometer spatial resolution. We observed the carrier generation by a laser pulse, deposition of energy into the lattice and ultra-fast (super-sonic) thermal expansion from 10 ps to 70 ps, and ensuing compression of the surrounding material from ~90 ps to ~250 ps. Heating and expansion resulted in a cavitation and void formation with a pressure wave started to propagate from ~250 ps. Subsequent thermal diffusion, re-flow and re-solidification of glass was followed in time up to 10 ns. A permanent refractive index modification after cooling was observed. From the sequence of these events, we know that the threshold energies required for the carrier generation and the pressure wave were almost the same, and the threshold energy of the permanent refractive index modifications was by ~40% larger. To the best of our knowledge, this is the first study allowing the threshold energy for laser processing to be decided based on the phase changes obtained from interference measurements. This method is useful because of a simple procedure and gives the threshold energy with high accuracy, high spatio-temporal resolution and sensitivity.

2. Experimental setup and procedure

2.1. Realization of counter-propagating pump-probe interferometry

Figure 1 shows the optical setup of a pump–probe interference microscope used in the experiments. The pump pulse with a center wavelength of $\lambda(\omega)$ = 800 nm generated by an amplified femtosecond laser system was focused inside a sample with a 100 × oil-immersion

#139857 - $15.00 USD Received 20 Dec 2010; revised 14 Feb 2011; accepted 28 Feb 2011; published 14 Mar 2011
(C) 2011 OSA

objective lens (OL) with an NA of 1.25. The sample was a borosilicate glass cover slip (Matsunami). The probe pulse was a second-harmonics of femtosecond laser pulse with a center wavelength of $\lambda(2\omega)$ = 400 nm generated in a barium borate (BBO) crystal. The probe pulse was irradiated onto the sample with a delay time T after arrival of the pump pulse and was introduced to the interferometer after passing through the sample. The delay T was controlled with an optical delay line with the maximum delay of 10 ns. Interference fringes were acquired with a cooled charge-coupled device (CCD) image sensor and read out by a computer for analysis. Resolution of the interferometric observation was 0.160 μm, which was calculated from a full width at half maximum (FWHM) of the Airy disk pattern obtained by focusing the illumination (probe) pulse of $\lambda(2\omega)$ using the 1.25NA objective lens; the magnification of the microscope, M, was 240 and the cut-off spatial frequency of the Fourier filtering h (described in the next section) was 19 line pairs per millimeter (lp/mm). In the framework of geometrical optics and with assumption of aplanatic optics, a computed cut-off frequency of the total system was Mh = 4500 lp/mm and the corresponding resolution limit was $1/Mh$ = 0.22 μm. This is slightly larger than the resolution limit of the microscope of 0.16 μm (FWHM) and was a bit smaller than the focal spot diameter of 0.33 μm (FWHM) for the 1.25NA and $\lambda(\omega)$.

Control of the pump pulse duration was made by an in situ monitoring the breakdown inside the glass and tuning an outside-cavity compressor: the lowest pulse duration at which the optical breakdown was observed was approximately 0.2 ps as measured by the fastest change of the phase at the focal spot; pulse duration at the laser output was 45 fs. The duration of the probe pulse was minimized by monitoring the most efficient SHG while pre-chirping pulse at the fundamental frequency. The coincidence T = 0.0 ps time between pump and probe was decided when there was no recognizable photomodification at the pump pulse of ~50 nJ; hence, when actual separation between counter-propagating pump and probe pulses was approximately equal to the pump pulse duration. Precision of the setting of the time reference frame was approximately ± 20 fs.

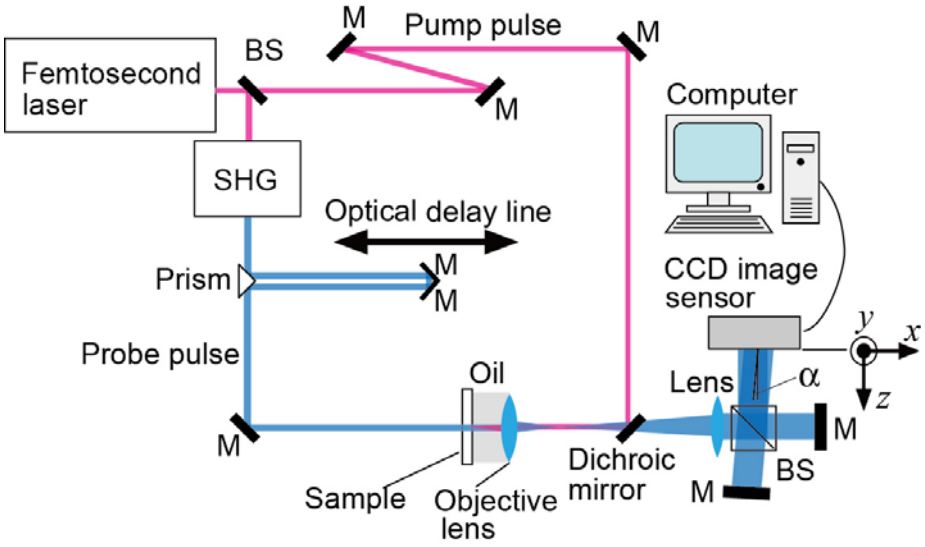

Fig. 1. Experimental setup: M - mirror, BS - beam splitter, SHG is the second harmonic generator, α is the angle between interferogram forming beams.

2.2. Image processing algorithm

A complex amplitude was calculated using the Fourier transform method [31]. The complex amplitude of an object wavefront on a CCD image sensor is described by

#139857 - $15.00 USD Received 20 Dec 2010; revised 14 Feb 2011; accepted 28 Feb 2011; published 14 Mar 2011
(C) 2011 OSA

$$U^{(S)}(x,y) = A(x,y)\exp\left[i\phi(x,y)\right], \tag{1}$$

where $A(x, y)$ and $\phi(x, y)$ are the amplitude and phase distributions, respectively. The reference wave, which is the same wave as the object wave tilted by an angle α in the x-z plane, is given by

$$U^{(R)}(x,y) = A(x',y)\exp\left\{i\left[\phi(x',y) + kx\sin(\alpha)\right]\right\}, \tag{2}$$

where $k = 2\pi/\lambda$, $x' = x/\sin(\alpha) - x_0$, and x_0 is the lateral displacement of $U^{(R)}$ relative to $U^{(S)}$.

Fringes formed on the CCD image sensor are defined as

$$\begin{aligned}\left|U^{(s)}(x,y)+U^{(R)}(x,y)\right|^2 &= \left|A(x,y)\right|^2 + \left|A(x',y)\right|^2 \\ &+A(x,y)A(x',y)\cos\left[\phi(x,y)-\phi(x',y)-kx\cos(\alpha)\right].\end{aligned} \tag{3}$$

If the maximum value of a spatial frequency $\mathbf{v} = (u, v)$ of $A(x, y)$ is smaller than $\mathbf{v}_c = \sin(\alpha)/\lambda$, the third term on the right-hand side of Eq. (3) can be separated from the other terms in the Fourier plane. The value of $\mathbf{v}_c$ was set at 23.5 lp/mm in the experiment. Therefore, $U^{(S)}(x, y)$ can be separated by a spatial Fourier filter. The filter $W(\mathbf{v})$ used in our experiments was of the Hanning type, described by

$$\begin{aligned}W(\nu) &= \left[1-\cos\left(\pi\left|\nu-\nu_c\right|/h\right)\right]/2, \quad if\ \left|\nu-\nu_c\right| \le h \\ &= 0, \qquad\qquad\qquad\qquad\quad \text{otherwise}\end{aligned} \tag{4}$$

where h is the filter width. Furthermore, if the spatial extents of $A(x, y)$ and $\phi(x, y)$ are smaller than $x_0/2$, then they can be separated in the image plane. Finally, the phase change $\Delta\phi$ is obtained by subtracting a phase distribution obtained without the pump pulse irradiation from the phase distribution measured with the pump pulse present.

3. Results and discussion

3.1 Time sequence of a cavity formation and relaxation

Figure 2 shows time-resolved images of the phase and amplitude calculated from the interference fringes along with temporal changes of the phase at points corresponding to the center of the irradiation pulse and at side-shifted locations [Temporal evolution of the phase is shown in Media1]. The real size of each image was 8.3 μm × 8.3 μm. The glass was irradiated with a laser pulse of E = 50 nJ energy (estimated at the focus), which was twice as high as the threshold of the carrier generation as described later. The positive $\Delta\phi$ indicated by a brighter shade corresponds to a negative refractive index change Δn, and the negative $\Delta\phi$ indicated by a darker shade corresponds to the positive Δn.

Let's discuss processes taking place at the center of irradiation spot and at 0.5 and 1.0 μm off-centered locations. At the center, the $\Delta\phi$ increased rapidly after the pulse irradiation, and reached 0.51π at T = 1.0 ps. This rise time depended on the pulse duration, and it was minimized to ~0.2 ps by pre-chirping of the pump pulse. The positive phase change occurs due to free-carrier generation via multiphoton and avalanche absorption. An estimation of the electron density can be done by comparison of the phase at the optical breakdown when electron density is 1.7 x 10^{21} cm^{-3} (critical plasma at 800 nm wavelength). Thermal ionization after the pulse also contributes to free carrier generation at larger pulse intensities [32]. The absolute value of the phase was not exactly determined due to a limited depth of the focus what causes saturation. The largest measured phase change at the center was approximately 0.84π at the breakdown. Then the central phase chance of 0.51π would correspond to electron density of 1.0 x 10^{21} cm^{-3}, hence, pre-critical plasma. The diameters of the phase change region at T = 0.5 ps and 1.0 ps appeared 0.55 μm and 0.66 μm at (FWHM), respectively. The excited area actually was smaller than the beam diameter of 0.33 μm (FWHM) due to the

#139857 - $15.00 USD Received 20 Dec 2010; revised 14 Feb 2011; accepted 28 Feb 2011; published 14 Mar 2011
(C) 2011 OSA

threshold effect and multiphoton character of the excitation. After fast phase increase due to free carrier generation at the center of irradiation spot, a plateau region followed (mainly due to saturation) with a slow change of carrier density due to recombination, which contributes to heating. The fast part of the recombination occurring during 0 - 1 ps has not been resolved.

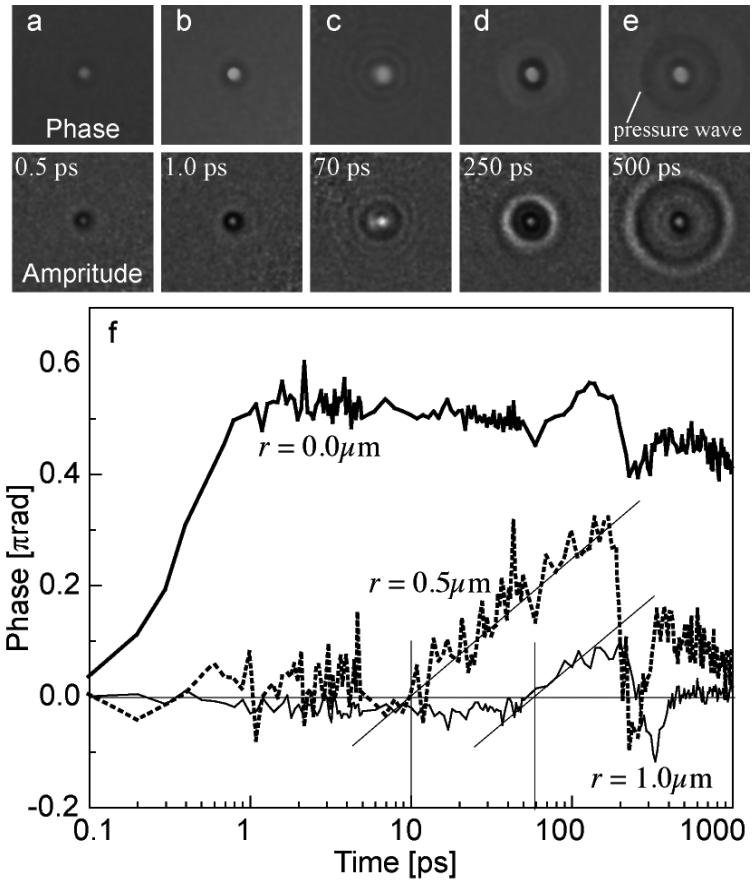

Fig. 2. Phase and amplitude of the probe pulse at T = (a) 0.5 ps, (b) 1 ps, (c) 70 ps, (d) 250 ps, and (e) 500 ps when E = 50 nJ. The image size was 8.3 μm × 8.3 μm. (f) Temporal changes of phase at focal point and points away from the focal point. r is the distance from the focal point. (Media 1)

At the location off-center shifted, a delay was observed in the onset of phase changes. A lateral increase of the positive phase change - as shown in Fig. 2(c) - was observed from ~10 ps at the 0.5 μm off-centered location. This indicates the thermal expansion delay as it arrives from the center of irradiated region where energy deposition from the photo-excited electrons to atoms/ions occurred, typically, within few picoseconds. In order to estimate speed of the process we compare arrival times at the two locations (0.5 and 1.0 μm out of the center). This comparison shows that expansion is super-sonic. The diameter of the positive phase change increased to 0.87 μm (FWHM) at the time moment of T = 70 ps.

As shown in Fig. 2(f), the increases in the phase at r = 0.5 μm and at r = 1.0 μm were observed from ~10 ps and from ~60 ps, respectively. From these results, the speed was estimated to be 1.0×10^4 m/s, which exceeded the acoustic velocity of 5.44×10^3 m/s in glass pointing out to the formation of the shock. Toward the end of the expansion recognizable as a phase increase at the observation points 0.5 and 1.0 μm apart from the center (f), a sudden decrease and sign reversal of the phase was observed as presented in (e, f). This fast phase change is consistent with a cavity formation in the heat-expanded volume as discussed next.

#139857 - $15.00 USD Received 20 Dec 2010; revised 14 Feb 2011; accepted 28 Feb 2011; published 14 Mar 2011
(C) 2011 OSA

At the end of the phase increase via expansion, an outward generation and propagation of the circular negative phase change, that is, a pressure wave, was observed. The same event was recognizable at the center ($r = 0.0$ μm) by the phase jump from $T = 180$ ps to 340 ps when inward propagation of the pressure wave can be observed in the phase images. These observations at the center and periphery of the irradiation site can be explained by the void cavity formation in the heated focal volume. When the pressure exceeds the surface tension of the shock molten glass the cavity bubble is formed – the phase reversal event resolved in (f). Similarity of irradiation conditions in terms of focusing and deposited energy used in these experiments and in a systematic study of breakdown in different glasses reported in Ref. 33 supports a conjecture of the glass melting during void formation. A mechanical 2D analogy of the cavitation is a string under tension; when it is cut in the middle a snapping (equivalent to cavitation) of the two loose ends takes place. In the case of the cavity formation inside a glass this would correspond to the free-surface compaction and subsequent relaxation. In the phase plot (f), this is seen as the positive index (negative phase) step-jump due to the compaction, which followed after a long ramp of heat expansion.

Further temporal evolution of the formed cavity was followed over longer time frame till 10 ns. The pressure wave propagated outward while decaying. The phase change decreased by 30% from $T = 350$ ps to 1 ns. As shown in Figs. 2(d), 2(e), the propagating speed was 5.40×10^3 m/s, which almost corresponds to the acoustic velocity. Finally, permanent positive refractive index change was formed at the focal point [see Fig. 4(c); details described below]. The positive index indicates a closure of the cavity formed earlier, most probably, by a melt re-flow as expected in the low melting temperature glasses [33,34].

Thermal expansion was an important step in the cavity formation. The temperature diffusion coefficient of borosilicate glass $\xi = 4.8 \times 10^{-7}$ m^2/s was directly measured [35]; the diffusion length was $L_d = (\xi \times 10 \text{ ns})^{1/2} = 70$ nm during 10 ns. Hence, a strong temperature localization and confinement were expected. The phase maps were sensitive to the local mass density around the irradiated spot. The density of glass (hence the local refractive index) was defined by the fictive temperature, T_f, and depends on the rate of heating/cooling of the glass/melt [36]. The cooling and glass-transition reflects kinetics of the mass density during glass solidification which occurs on a microsecond time scale and has a complex pattern of viscous flow, compaction, and stress distribution in the presence of void [34,37]. At different positions from the irradiation point the density of glass has to be different due to different cooling rates (hence, glass of different fictive temperature will be formed). The proportionality between the density and fictive temperature, which has never been investigated at such extreme thermal heating/quenching rates when a femtosecond pulse is used, still has to be established.

Earlier studies of cavity formation in glasses by femtosecond laser pulses were performed under multi-pulse irradiation conditions with heat accumulation [34,37] and showed a complex mass density dynamics as revealed by front [34] or side imaging [37]. The focusing used in those studies was less tight as compared to this work and the cavitation was driven by the multi-pulse heat accumulation. When tight focusing is used, a side imaging with a high numerical aperture lens is impossible. It has been observed that in materials with very high melting temperature such as sapphire, quartz, pure silica glass, a void can be formed at lower pulse energy due to limited reflow [32,33]. Modeling [32,38] of void formation at tight focusing conditions can be explained by shock compression; it is noteworthy that the void is still present after all the relaxations. The current pump-probe experiments showed more complex dynamics inside borosilicate glass, when cavitation can be formed by a single laser pulse but latter the void is reflown by the molten phase. The presented time-resolved pump-probe analysis of the processes occurring at the focal volume can be extended to different materials and yield in more details about cavitation in materials under tight focusing.

#139857 - $15.00 USD Received 20 Dec 2010; revised 14 Feb 2011; accepted 28 Feb 2011; published 14 Mar 2011
(C) 2011 OSA

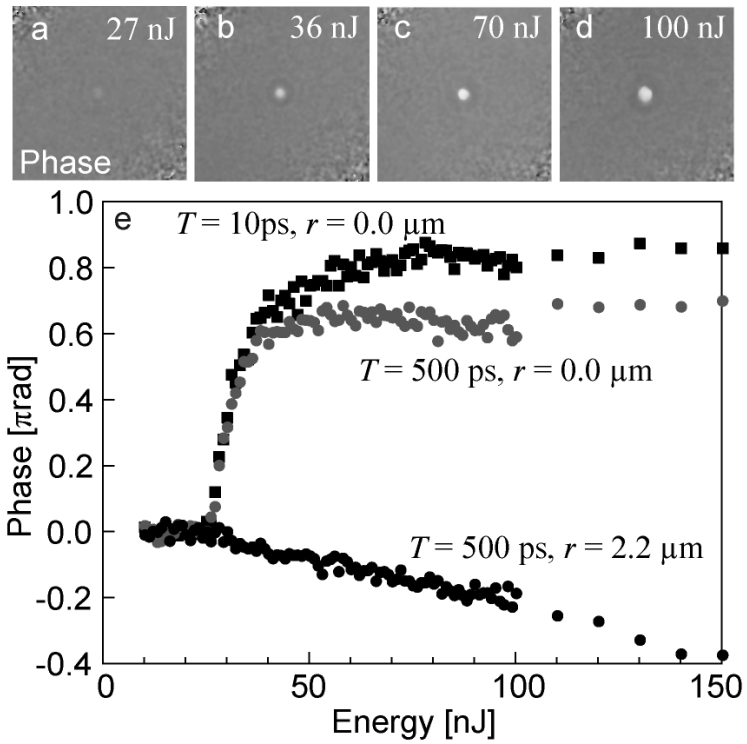

Fig. 3. Phase images at T = 10 ps when the pulse energy was (a) 27 nJ, (b) 36 nJ, (c) 70 nJ, and (d) 100 nJ, respectively. The image size was 13.3 μm × 13.3 μm. (e) Phase changes at the pulse irradiation point versus energy E. T is the delay time, and r is the distance from the focal point.

3.2. Power dependence of the light-matter interaction

Figure 3 shows phase distributions under laser pulse irradiation with energy E = 27, 36, 70, and 100 nJ at T = 10 ps, together with the phase change versus E at the center and r = 2.2 μm away from the center. The images had an actual size of 13.3 μm × 13.3 μm. For the respective energies, the diameters of the phase changes were 0.48, 0.61, 0.78, and 0.89 μm (FWHM), and the center phase changes were 0.12π, 0.61π, 0.82π, and 0.80π. A positive phase change at r = 0 appeared from E = 24 nJ, rapidly increased to E = 36 nJ, and then saturated. The saturation of the phase change can be explained by an increasing axial length of the phase change region in excess of the focal depth of the objective lens (0.192 μm). The rapid phase change from 24 to 36 nJ was caused by not only an increase in the diameter of the carrier generation but also by an increase in the axial length. When the irradiation energy E was changing from 24 to 35 nJ, the characteristic phase changes from T = ~70 ps to 340 ps and the generation and propagation of a pressure wave were not observed (the expansion stage). A negative phase change (T = 500ps, r = 2.2μm) caused by a pressure wave appeared from E = 32 nJ (the phase flip due to the cavitation). The phase change linearly decreased with increasing E because the width was larger than the resolution limit (0.22 μm FWHM). From linear regression around the threshold value, the threshold energies for generation of free carrier and pressure waves were estimated to be the same and occurred at 24 nJ. This interferometric observation of laser induced phenomena gives the exact threshold values for the refractive index changes in glass revealed by the analysis of the phase image.

Figure 4 shows phase and amplitude images of the permanent structure and power dependence of phase at the center. When E was 30 nJ, no permanent structure was formed. At 35 nJ, a small permanent refractive index change was formed, as shown in Fig. 4(b) and the amount of permanent refractive index change increased with increasing E, as shown in Figs.

#139857 - $15.00 USD Received 20 Dec 2010; revised 14 Feb 2011; accepted 28 Feb 2011; published 14 Mar 2011
(C) 2011 OSA

4(c), 4(d), and 4(e). The center phase also decreased according to the increase in E (Fig. 4(f)). The threshold energy of the permanent refractive index change was estimated to be 35 nJ from the linear regression line. It has not been reported before that the threshold of the permanent refractive index formation (35 nJ in our experiments) was different from the threshold energies of the free carrier generation and the pressure wave generation that we determined to

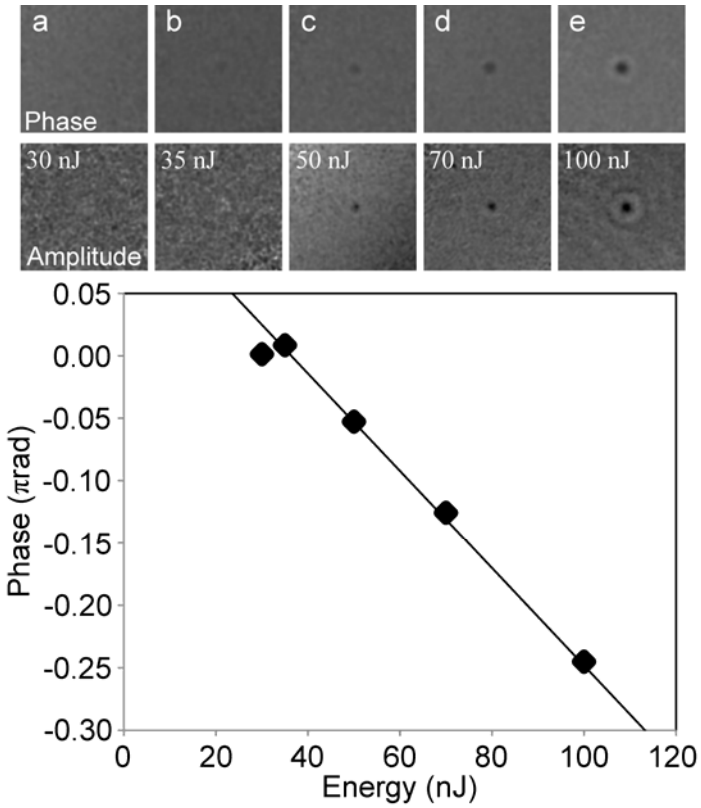

Fig. 4. Phase and amplitude images of the permanent structures. The pulse energies were (a) 30 nJ, (b) 35 nJ, (c) 50 nJ, (d) 70 nJ, and (e) 100 nJ, respectively. The image size was 8.3 μm × 8.3 μm. (f) Phase changes of the final structures versus energy E.

take place at 24 nJ for our experimental conditions. The energies from 24 to 35 nJ would perform an excitation of materials without permanent structural changes in borosilicate glass. If the pulse energy is below the threshold of the cavitation (35 nJ), then the induced optical modifications recover after thermal relaxation.

4. Conclusions

We demonstrated the method to follow the spatiotemporal evolution of carriers excited by a femtosecond laser pulse, heat expansion, a pressure wave, cavitation, shock formation and the final heat diffusion and cooling from 100 fs to 10 ns using temporal phase images obtained by time-resolved pump–probe interferometry. We found that the free carrier generation and thermal expansion have comparable threshold energies. The permanent refractive index modifications were observed only when this threshold energy was increased by approximately 40% and the cavitation occurred. The experiments were conducted near the threshold energy because it is important for many applications to make modifications and refractive index changes with sub-wavelength feature size achievable at the close-to-the-threshold conditions. We found that even in the case of sub-critical plasma, the cavitation can be induced in

#139857 - $15.00 USD Received 20 Dec 2010; revised 14 Feb 2011; accepted 28 Feb 2011; published 14 Mar 2011
(C) 2011 OSA

borosilicate glass due to localized heating but the void closes on a later stage of relaxation by melt reflow.

The femtosecond laser pulse irradiation at the near breakdown threshold energy is expected to become a powerful tool for creating new three-dimensional functional nanostructures in transparent materials such as glasses, crystals, semiconductors, polymers, and biomaterials. The highly sensitive and quantitative interferometric measurements will provide informative and quantitative characterization of the physical phenomena occurring after ultra-fast energy delivery by femtosecond-laser pulses. The presented method can be adopted for characterization of femtosecond-laser structuring by pulses of complex amplitude and phase distributions such as Bessel and optical vortices. The revealed stages of fast expansion due to heating with subsequent cavitation could explain recently observed large volume ablation of glass when femtosecond Bessel pulses were used [39].

Acknowledgements

This work was supported by The Murata Science Foundation, The Asahi Glass Foundation, The Amada Foundation for Metal Work Technology, and a Grant-in-Aid for Scientific Research (B) from the Ministry of Education, Culture, Sports, Science and Technology of Japan.

#139857 - $15.00 USD Received 20 Dec 2010; revised 14 Feb 2011; accepted 28 Feb 2011; published 14 Mar 2011
(C) 2011 OSA